

Article

Capacitive and Non-Contact Liquid Level Detection Sensor Based on Interdigitated Electrodes with Flexible Substrate

Yong Ren, Bin Luo, Xueyu Feng, Zihao Feng, Yanyi Song and Fang Yan *

School of Microelectronics and Communication Engineering, Chongqing University, Chongqing 401331, China; renyong@cqu.edu.cn (Y.R.); 202312131100t@stu.cqu.edu.cn (B.L.); 202312131037t@stu.cqu.edu.cn (X.F.); 202312131071t@stu.cqu.edu.cn (Z.F.); songyanyi@cqu.edu.cn (Y.S.)

* Correspondence: yanfang@cqu.edu.cn

Abstract: Achieving accurate and high-sensitivity liquid level detection in medical instruments has always been a knotty task. In this paper, a high-precision, non-contact, flexible capacitive liquid level sensor is proposed, aiming to apply capacitive sensors in test tube liquid level measurement and improving the sensitivity of real-time liquid level sensors. The simulation study is conducted using ANSYS Maxwell and demonstrates the correlation between test tube thickness and sensitivity. A geometric model of the test container and sensing electrodes is established to optimize the design strategy for the physical dimensions of the sensor's interdigitated (IDT) electrodes based on a flexible printed circuit (FPC). The hardware and software designs are completed based on the FDC2214 capacitive-to-digital converter to collect the capacitance variation data of the sensing electrodes accurately. To assess the system's performance, an experimental platform for a liquid level sensor system has been constructed, facilitating the measurement, communication, processing, and visualization of liquid levels. The performance results demonstrate that the system is capable of accurately measuring the effective liquid level range within a standard 5 mL test tube with a resolution of up to 1 mm, as well as a sensitivity of 78.68 fF/mm, verifying the simulation results and exhibiting excellent linearity.



Citation: Ren, Y.; Luo, B.; Feng, X.; Feng, Z.; Song, Y.; Yan, F. Capacitive and Non-Contact Liquid Level Detection Sensor Based on Interdigitated Electrodes with Flexible Substrate. *Electronics* **2024**, *13*, 228. <https://doi.org/10.3390/electronics13112228>

Academic Editor: Marcin Witczak

Received: 15 May 2024

Revised: 1 June 2024

Accepted: 5 June 2024

Published: 6 June 2024



Copyright: © 2024 by the authors. Licensee MDPI, Basel, Switzerland. This article is an open access article distributed under the terms and conditions of the Creative Commons Attribution (CC BY) license (<https://creativecommons.org/licenses/by/4.0/>).

Keywords: capacitive liquid level sensor; fringing field; interdigitated (IDT) electrodes; FDC2214

1. Introduction

The principle of liquid level detection technology is to detect changes in the liquid level of the measured liquid via corresponding changes in easily detectable electrical signals, thereby converting the physical quantity change into a detection signal. Nowadays, liquid level measurement technology is widely used in various industries, such as healthcare [1,2], agricultural monitoring [3], aquarium [4], and the petrochemical industry [5,6]. Especially in medical instruments, liquid level detection is a critical component of IVD (in vitro diagnosis) instruments, such as the blood detector, the immune system analyzer, the urine analyzer, and others [7], all of which directly influence the accuracy and safety of automated detection in medical instruments.

Currently, liquid level detection technology can be divided into two main categories based on whether the sensor makes direct contact with the liquid: contact methods and non-contact methods [8]. Existing contact-based liquid level detection technologies include (1) the resistive method [9], where the resistance changes as two electrodes contact conductive liquid when the liquid level drops with a moving liquid needle; this method has a simple structure and low-cost advantages, but its drawbacks include high power consumption and the inability to detect non-conductive liquids; (2) the capacitive probe method [10], where the capacitance sharply increases when the probe contacts the sample, with low cost and wide application but insufficient resistance to abnormal interference; (3) the capacitive submerged method [11,12], which uses sensors submerged in liquid with different structures (such as parallel, coaxial cylinder, helical, etc.) to achieve higher

sensitivity on capacitance; (4) and the optical fiber method [13], which measures the liquid level by monitoring the interference and refraction of light in optical fiber. However, contact-based methods require electrodes to be in contact with the liquid for an extended period, leading to an increase in the risk of contamination or oxidation and reducing detection accuracy and reliability. Also, this type is unsuitable for liquids with high viscosity and highly chemically reactive materials, such as paints and highly reactive chemicals. Non-contact methods include (1) the ultrasonic method [14,15], which measures the liquid level by timing how long it takes for sound waves to reflect off the water surface and return; (2) the microwave method [16], which is based on the principles of electromagnetic waves, measuring the liquid level by monitoring the propagation characteristics of microwave signals in different media (El-Nady, S. et al. proposed a combination of ENZ metamaterials and aperture amending and detected the concentration of sugar and salt in water with high resolution and sensitivity [17]); and (3) the acoustic resonance method [18], which based on sound reflection phenomena and detects a group of resonance frequencies (RFs) to calculate the liquid level. However, sensors in these methods are relatively expensive, and ultrasound or active microwave methods may pose risks of chemical reactions leading to the container's breakage of liquid or cellular components [19]. Efforts have been made to utilize machine vision and neural networks [20,21] as a new liquid level detection system. However, it is noteworthy that this method is accompanied by challenges such as intricate spatial deployment, considerable hardware expenditure, and a requirement for container transparency.

The capacitive method, a classic non-contact method, employs a sensing electrode configuration to detect changes in liquid level height through capacitance variation. This method offers a simple structure, low cost, and no liquid contamination. T. Islam et al. proposed an improvement to the liquid level sensing sensitivity by changing the ratio of the working electrode to the sensing electrode in the IDT electrode structure. This resulted in a sensitivity of 39.8 fF/mm and a range of 0–40 mm, as proven by FEM simulation and experiment [22]. S. Ahmad et al. proposed an interdigitated capacitive sensor based on coplanar waveguide feed for efficient power transfer, with the capacitive sensitivity of 7.5 fF/%WC, 4.5 fF/%RH, and 13.4 fF/mm for soil moisture, air humidity, and water level detection, respectively [23]. Qian, Z et al. proposed a carbon nanotube composite single-electrode capacitive sensor to improve SNR. It resulted in a dynamic range of 400 mm, with a resolution of 1.1 mm and 6.5 fF/mm [24]. This non-contact level detection method based on IDT electrodes has been studied and improved by many scholars. These studies have engaged in the exploration of novel sensing materials and the fine-tuning of sensor architecture and have resulted in notable advancements. Nevertheless, these methodologies have not yet reached the desired level of sensitivity.

A comparison of the proposed sensing method with other liquid level detection sensors is given in Table 1.

Table 1. Comparison of the developed sensor with other related liquid level sensors.

Reference	[12]	[25]	[24]	[26]	[27]	This Work
Measurement Type	Capacitive contact	Capacitive non-contact	Capacitive non-contact	RFID Contact/Non-contact	Capacitive non-contact	Capacitive non-contact
Sensing structure	Helical	FPC	Single electrode	IDT Rogers	1-3-1 IDT FR4	IDT FPC
Range (mm)	600	900	400	20	40	40 or higher
Resolution	2 cm	0.2 mm	1.1 mm	/	0.1 mm	1 mm
Sensitivity	701.6 nF/mm	0.012 V/mm	6.5 fF/mm	2.15 °/mm	40 fF/mm	78.68 fF/mm
Application scenarios	Water tank	Clinical infusion	Water level and rain detection	Wireless	Water tank	Test tube

This study proposes a novel design method for a non-contact capacitive liquid level sensor based on flexible IDT electrodes to further increase the sensitivity. First, the principle of liquid level measurement based on capacitance is elaborated, starting from the fundamental principles of coplanar capacitors and fringing fields. Then, Maxwell 3D in ANSYS Electronics Desktop 2023 is utilized for modeling and simulation optimization to design high-sensitivity IDT electrodes based on a flexible printed circuit board (FPC). Subsequently, a high-precision capacitance-measuring-instrument-based FDC is developed, and the LCR meter is compared in tests to verify its high accuracy for pF-level capacitance measurement. The experimental results demonstrate that the proposed liquid level detection sensor exhibits several advantages, including low cost, non-contact operation, flexibility, and high sensitivity of 78.68 fF/mm with linearity of 1.6%. Furthermore, this proposed method has the potential to be applied to a wider range of medical instruments.

2. Theory

Under ideal circumstances, electric field lines typically exist within the dielectric between two parallel conductor plates, oriented vertically from the positive electrode to the negative electrode. However, practical considerations introduce curvature to the electric field lines at the edges due to edge effects. As the plates gradually expand outwards until they are coplanar, the electric field lines in the space gradually diverge due to these edge effects [22,28]. This process is simulated and demonstrated as shown in Figure 1. The coplanar structure electrodes enable the examination of material under test (MUT) from only one side. This is especially beneficial when there is a restriction for accessing both sides of the MUT, such as covering coplanar electrode capacitors on ice-covered insulators to predict flashover risk [29].

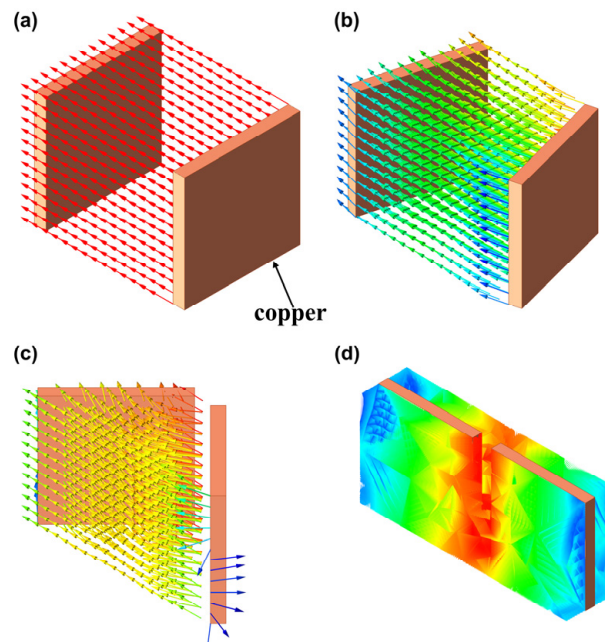


Figure 1. Transition of a parallel to a coplanar copper electrode capacitor (the colors in the figure reflect the electric field intensity and follow the distribution of a rainbow): (a) ideal parallel electrode capacitor; (b) e-vector in open transition with copper electrodes opening angle of 30 degrees; (c) e-vector in open transition with copper electrodes opening angle of 90 degrees; (d) Mag-E in coplanar electrode capacitor.

Theoretically, the mathematical formula for the electric field Gauss's law in Maxwell's equations is given by

$$\nabla \cdot D = \rho_{\Omega}, \quad (1)$$

where ρ_Ω is the volume charge density within the volume Ω , and D is the electric displacement vector, respectively. Substituting the relationship between the electric displacement vector and the electric field intensity in the electrostatic field, $D = \epsilon_0 \epsilon_r E$, into Equation (1):

$$\nabla \cdot (\epsilon_0 \epsilon_r E) = \rho_\Omega, \quad (2)$$

where ϵ_r is the permittivity distribution function in three-dimensional field space, and ϵ_0 is the permittivity of free space. Applying $E = -\nabla \Phi$ (the electric field is the negative gradient of the electric potential) to Equation (1), where Φ is the potential distribution function in field space, is given as follows:

$$\nabla \cdot (\epsilon_0 \epsilon_r \nabla \Phi) = -\rho_\Omega. \quad (3)$$

Assuming no free charge exists within the region Ω , the static electric field within the area can be characterized by Laplace's Equation [30,31]:

$$\nabla \cdot (\epsilon_0 \epsilon_r \nabla \Phi) = 0. \quad (4)$$

Solving Equation (4) for Φ numerically by specifying the boundary conditions yields the potential distribution function within the three-dimensional field. Subsequently, the capacitance value can be computed by employing the capacitance calculation formula, written as follows:

$$C = \frac{Q}{V_\Omega} = \frac{\int_\Omega D d\Omega}{V_\Omega} = \frac{\int_\Omega \epsilon_0 \epsilon_r (-\nabla \Phi) d\Omega}{V_\Omega}. \quad (5)$$

Equation (5) demonstrates that capacitance is not solely contingent upon the spatial distribution of permittivity but also intricately tied to the potential distribution. Nonetheless, obtaining its solution poses formidable challenges, necessitating the utilization of three-dimensional finite element software for accurate computation.

There are various options for sensing electrode structure, including cylindrical, coaxial, parallel, and coplanar configurations. Considering their application on the walls of test tubes, rigid PCB boards based on FR4 substrate cannot be utilized. Instead, flexible PCB (FPC) is preferred to better conform to the test tube wall, potentially enhancing sensitivity. The interdigital (IDT) sensing electrodes discussed below belong to the coplanar category, which offers a non-invasive, high-SNR, and single-sided measurement of the tested samples. The structure of IDT trumps other electrode structures for designing the sensor device due to its low cost, ease of fabrication process, and excellent sensitivity [22,32].

The structure of interdigital electrodes dictates the direction of electric field lines under the influence of fringing fields, which propagate from the working electrode (WE) towards the sensing electrode (SE). The WE and SE collectively form a pair of IDT structures. The presence of the MUT within the electric field alters its dielectric properties, resulting in a change in capacitance between the IDT electrodes. Due to this characteristic, interdigital capacitive sensors have wide applications in chemical sensors, strain gauges, food inspection, humidity sensors, biosensor applications, and concrete moisture content measurement [33,34].

The common interdigital electrodes feature an alternating arrangement of working and sensing electrodes while maintaining equal spacing between the two electrodes. The repeated nature of the electrodes causes a more robust signal than those gained by only one pair of electrodes. A simplified structure is shown in Figure 2. This configuration of uncomplicated IDT electrodes offers exceptional sensitivity for measuring fringing fields.

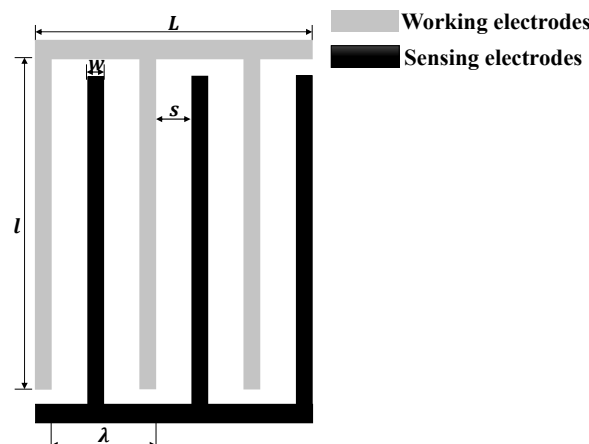


Figure 2. Diagram of IDT electrode structure.

w and l are the width and length of the interdigital electrodes shown in Figure 2, respectively; and s is the gap or spacing between adjacent pairs of interdigitated fingers. In general, all interdigital fingers are horizontally arranged with equal spacing. The metalization ratio η is the ratio of w to $w + s$; and λ is the wavelength or the periodicity of electrodes, which can be expressed as $\lambda = 2(w + s)$. A cross-sectional view of the IDT electrodes is provided in Figure 3.

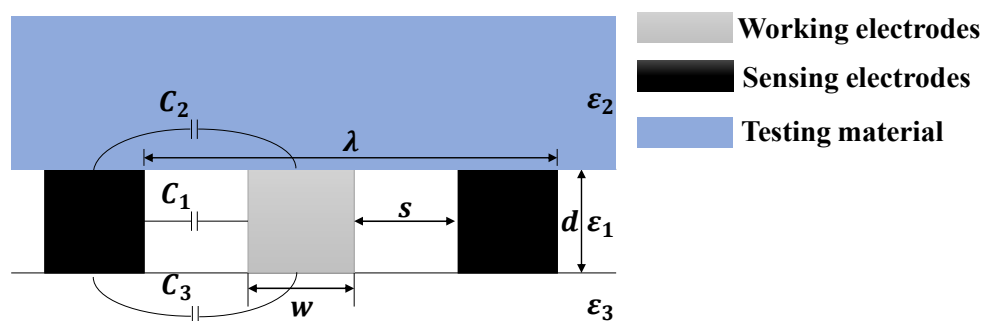


Figure 3. Top view and cross-sectional of IDT electrode.

d is the thickness of the interdigital fingers. For a pair of interdigital electrodes, the capacitance $C_0 = C_1 + C_2 + C_3$, where C_1 denotes the capacitance between the interdigital fingers, C_2 represents the capacitance caused by the edge effect of the MUT, and C_3 indicates the capacitance generated by the edge effect of the substrate. Calculating C_1 is relatively straightforward using the formula for parallel plate capacitors, but determining C_2 and C_3 is more complex. The two-dimensional distribution of the electric field for a pair of semi-infinite electrodes can be solved with conformal mapping techniques using an inverse cosine transform [35]. The electrode capacity of this geometry can be calculated as follows:

$$C = \frac{2\epsilon_0\epsilon_r l}{\pi} \ln \left[\sqrt{\left(1 + \frac{2w}{s}\right)^2 - 1} + \left(1 + \frac{2w}{s}\right) \right]. \quad (6)$$

Equation (6) estimates the self-capacitance value of a pair of coplanar electrodes with finite width ($w/g \gg 1$). The combined effect of the medium's dielectric constant and the electrode's physical geometric size affects the overall capacitance value.

The capacitance sensitivity S is defined as the degree to which the capacitance changes with variations in the physical properties of the MUT, such as dielectric constant or shape. In applications such as liquid level detection, it can be expressed as follows:

$$S = \Delta C / \Delta h, \quad (7)$$

where ΔC is the change in capacitance; and Δh is the corresponding change in the height of the liquid level. A higher sensitivity indicates that the sensor's capacitance value is more responsive to changes in the liquid level and is less susceptible to specific external influences. Consequently, this study primarily examines the influence of the diverse physical dimensions of interdigital electrodes based on flexible substrates on the sensitivity of the sensor output.

3. IDT Simulation and Design

The range and sensitivity of the sensor can be modified by adjusting the dimensions of the electrodes [36]. Consequently, given the complexity of the coplanar capacitance formulae, finite element analysis software is employed for the simulation, solver, and investigation of electrostatic field solutions of interdigital electrodes with different physical dimension parameters. The objective of this approach is to enhance sensitivity. The ANSYS Electronic Desktop 2023 and its Maxwell are employed to model and simulate the various geometric dimensions of the electrodes and thickness of test tubes.

The test tube employed is a standard 5 mL glass tube with the following dimensions: diameter 10 mm, height 75 mm, and wall thickness 0.9 mm. The material is glass, with a relative permittivity of 5.5. The dimensions of the testing electrodes are fixed at 16 mm in width and 42 mm in height, with a height of 1 mm at the connection point. The solution under investigation in the test tube is pure water, and the relative permittivity in the simulation environment is set to 81.

The first consideration is a set of parameters on the plane, namely, the interdigital electrode's lateral width ($x_0 = w$) and longitudinal length ($y_0 = l$). Figure 4 shows that these lengths are (1, 39) and (1.5, 39.5) in millimeters, respectively. Also, Figure 4c,d indicate the simulation model with different sizes of IDT electrodes. The IDT electrode adhering to the test tube is at a height of 14 mm above the circular bottom of the cylinder of the test tube. The thickness of the copper foil is 1 OZ (0.035 mm).

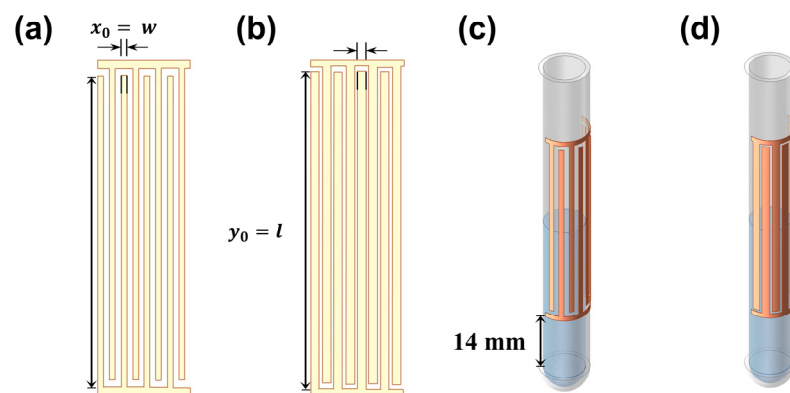


Figure 4. Model of IDT electrode with two kinds of structure in plane: (a) $x_0 = w = 1$ mm, $y_0 = l = 39$ mm; (b) $x_0 = w = 1.5$ mm, $y_0 = l = 39.5$ mm; (c) glass tube model with IDT size in (a); (d) glass tube model with IDT size in (b).

In general, after constructing the model in the software, the solution domain is defined as a three-dimensional space, including the test tube. The excitation of the IDT working electrode is set to 1 V, while the sensing electrode is set to 0 V. The adaptive mesh is set to enhance the efficiency and accuracy of the simulation solution. The scanning interval and step size are incorporated into the electrode dimensions parameters before the simulation, and the data are exported and analyzed after the simulation.

Considering the actual manufacturing process with a minimum gap of 4 mil, the simulation step size is set to 0.1 mm. This corresponds to electrode lateral metalization ratios ranging from 50% to 90% and longitudinal metalization ratios ranging from 90% to 99%. The simulation of the interdigital electrodes under a 1 V excitation voltage is depicted in Figure 5.

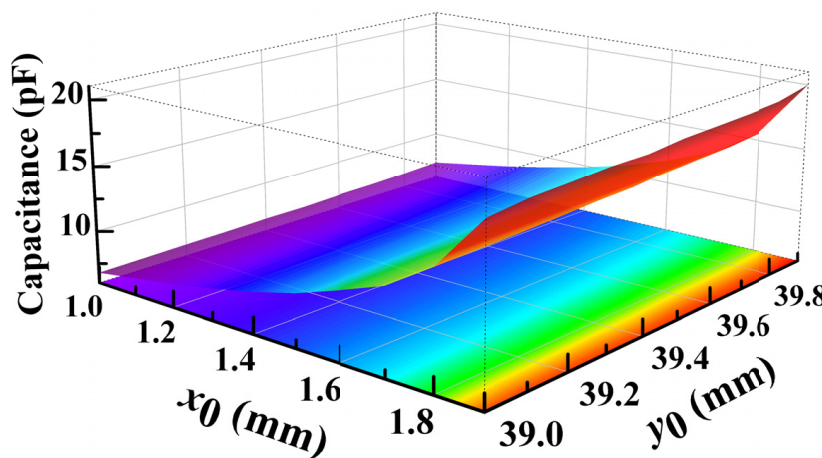


Figure 5. The influence of IDT electrodes' lateral and longitudinal metalization on capacitance.

It can be observed in Figure 5 that as x_0 and y_0 increase, the capacitance of the electrodes also increases, ranging from a minimum value of 6.79 pF to a maximum value of 20.01 pF. This observation aligns with Equation (1). However, the effect of the longitudinal metalization ratio on the capacitance of the electrodes is relatively small compared to the lateral metalization ratio. Therefore, it is considered to set both the lateral and longitudinal metalization ratios to 90%, corresponding to (1.9, 39). Six sets of data were simulated for practical applications, corresponding to electrode dimensions of (1, 39), (1.5, 39), (1.5, 39.5), (1.9, 39), (1.9, 39.9), and (1.8, 39.9), respectively, for liquid level heights ranging from 10 mm to 60 mm. The scatter plot of capacitance values at different liquid levels h_0 and the fitting lines obtained using the least squares method are shown in Figure 6.

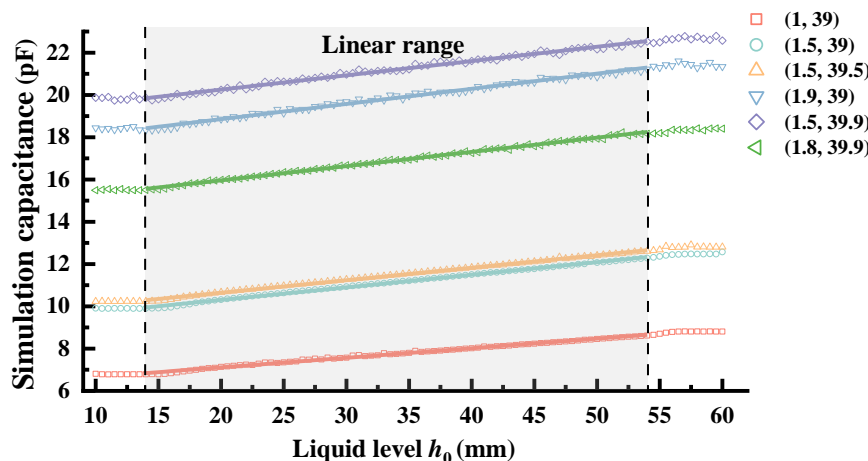


Figure 6. Capacitance values in the form of simulation point data and fitting lines with respect to the liquid level for six kinds of IDT sensors.

The capacitance value is observed to increase proportionally with the rise in liquid level h_0 , exhibiting good linearity when the liquid level is situated between the upper and lower edges of the sensing electrodes. The simulation also demonstrates that the parasitic capacitance between the liquid to be measured and the sensing electrodes exhibits a correlation with the height of coincidence between them. This implies that the height of coincidence between the liquid to be measured and the sensing electrode plate is proportional to the capacitance formed between them. Following the extraction of the measurement range, the slope and absolute mean error of the fitting line, ranging from 14 mm to 54 mm, are presented in Table 2.

Table 2. Fitting result for three kinds of (x_0, y_0) .

(x_0, y_0)	Slope (fF/mm)	R^2	Mean Error (fF)
(1, 39)	45.2	0.99466	0.32218
(1.5, 39)	59.5	0.99875	0.33871
(1.5, 39.5)	59.1	0.99798	0.29075
(1.9, 39)	71.8	0.99082	0.81483
(1.9, 39.9)	67.6	0.99011	0.78857
(1.8, 39.9)	67.3	0.99678	0.44146

The small error induced by the fitting is evident from the R-square. Additionally, when the parameters are set to $(x_0, y_0) = (1.9, 39)$, the maximum slope is performed, indicating the highest sensitivity. The corresponding distribution of the electric field intensity is illustrated in Figure 7.

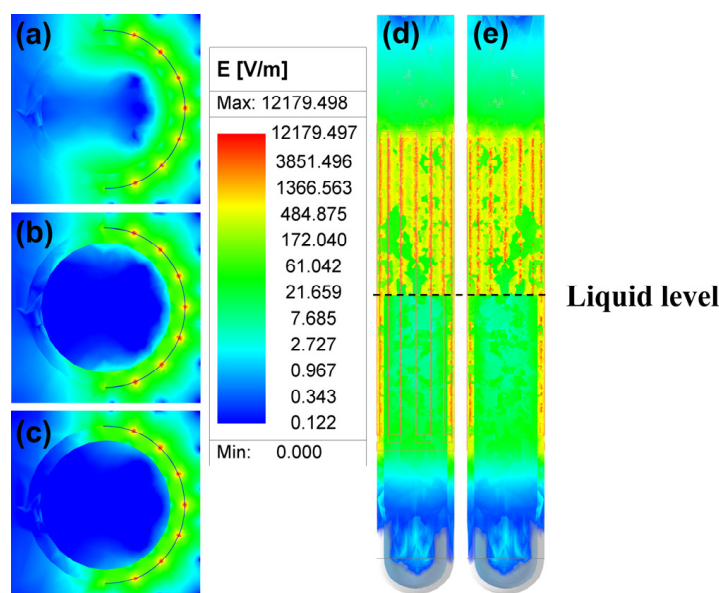


Figure 7. Electrical field distribution of the sensor in the glass tube with water (a) from a cross-sectional (liquid level above 1 mm) perspective; (b) from a cross-sectional (liquid level) perspective; (c) from a cross-sectional (liquid level below 1 mm) perspective; (d) from a frontal perspective; (e) from behind.

The spatial electric field line generated by the working electrodes, as shown in Figure 7, entered the water through the glass from the front, passed through the glass from the other side, and finally reached the sensing electrode. The distribution of the electric fields in water and air is significantly different. The fringing electric field is heterogeneously distributed between the electrodes and causes changes in capacitance, which was referred to in Equation (5).

In addition, considering the limitations imposed by the most extreme manufacturing processes on the impact of the wavelength $\lambda = 2(w + s)$ on the sensitivity, three sets of values are selected for comparison. These values are 1 mm, 2 mm, and 4 mm. It is worth noting that previous discussions on other factors related to the IDT electrodes were conducted under the assumption of $\lambda = 4$ mm. The results of the linear fitting calibration curves for the IDT electrodes with a width of 16 mm, a height of 40 mm, and h_0 ranging from 14 mm to 54 mm are shown in Figure 8.

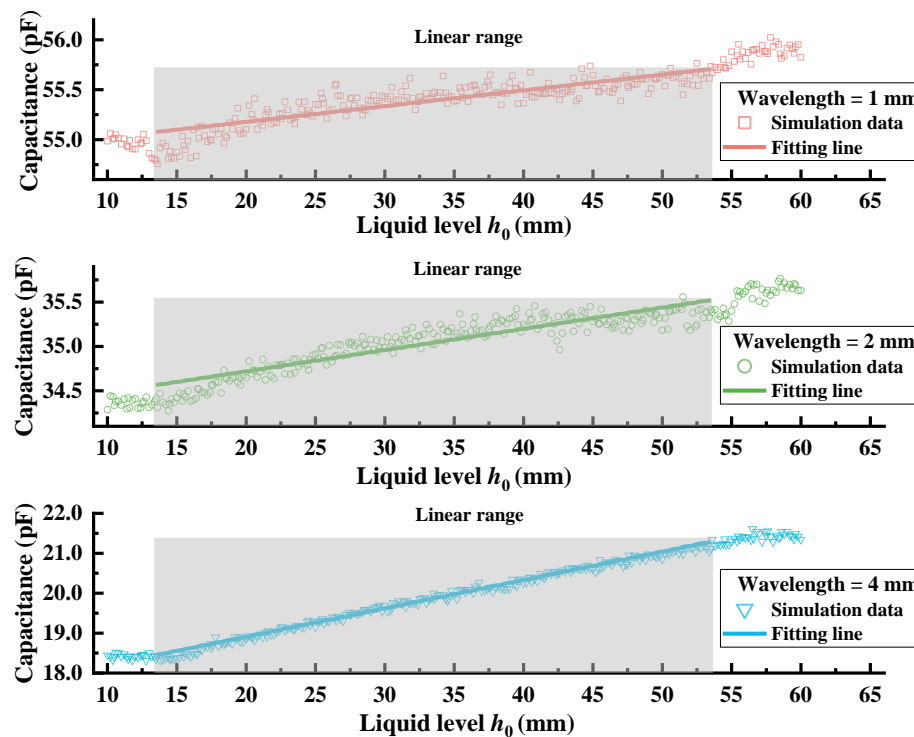


Figure 8. Capacitance values in the form of simulation point data and a fitting line with respect to the liquid level for three kinds of IDT wavelength (1 mm, 2 mm, and 4 mm).

The relevant parameters of the linear fitting for Figure 8 are shown in Table 3, where N is the number of fingers.

Table 3. Fitting result and relevant parameters for three kinds of λ .

λ (mm)	w (mm)	s (mm)	N	Slope (fF/mm)	R^2
1	0.4	0.1	32	15.8	0.75798
2	0.9	0.1	16	23.95	0.83988
4	1.9	0.1	8	71.06	0.99116

It is evident that as the IDT wavelength decreases at different wavelengths, the intrinsic capacitance during measurements increases. However, the slope or sensitivity of the capacitance with respect to the rising liquid level decreases, and the R-square value also declines sharply. Consequently, at an IDT wavelength of 4 mm, it can be considered a relatively suitable value under the experimental conditions.

The effect of glass test tube wall thickness on capacitance sensitivity is studied based on Equation (5). It can be observed that at a given volume, a thinner glass test tube wall results in a larger water volume within the capacitive sensing range. Additionally, the dielectric constant of water is considerably higher than that of glass, which enables the attainment of enhanced sensitivity. As shown in Figure 9, the simulation results corroborate this hypothesis. When the thickness of the test tube is 0.5 mm, the sensitivity reaches 222.9 fF/mm, which is three times the sensitivity of a test tube with a standard thickness of 0.9 mm. Nevertheless, the production of thinner-gauge tubes remains a significant challenge in terms of both material science and manufacturing processes.

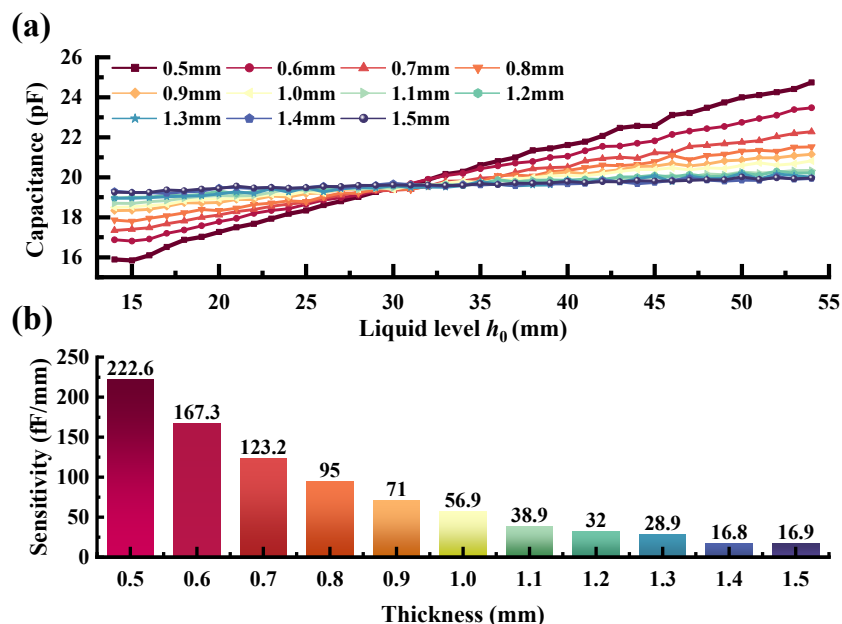


Figure 9. (a) Simulation capacitance with respect to liquid level for different thicknesses of the test tube; (b) sensitivity.

The physical dimensions of the IDT were researched and determined. Subsequently, an FPC (flexible printed circuit) adhering to manufacturing processes was designed using EasyEDA (<https://easyeda.com/>), that is an Electronic Design Automation (EDA) software. The FPC is a single-layer board with a thickness of 0.11 mm and copper thickness of 0.035 mm, with a flexible substrate made of polyimide (PI). Samples manufactured by the JLCPCB factory in Shenzhen, China, as shown in Figure 10, exhibit a mature production process for the FPC. This process is well-suited to mass production and offers competitive manufacturing costs. The design also incorporates solder pads on both sides to facilitate soldering.



Figure 10. Fabricated IDT electrode with flexible substrate.

4. Design and Fabrication of Capacitor Measurement

A simple series RLC circuit is depicted in Figure 11.

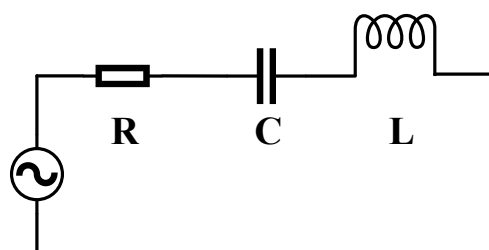


Figure 11. Diagram of RLC series circuit.

The total impedance is given by

$$Z = R + j \left(2\pi f_0 - \frac{1}{2\pi f_0 C} \right). \quad (8)$$

To maximize the current flowing through the entire circuit, we aim to minimize the total impedance with $\text{Im}\{Z\} = 0$. Thus,

$$f_0 = \frac{1}{2\pi\sqrt{LC}}. \quad (9)$$

When resonance occurs in the series RLC circuit, denoted by f_0 , which serves as both the natural and resonance frequency of the circuit, the task transitions from directly measuring the capacitance to determining the circuit's resonance frequency with the inductance known. The FDC2x1x capacitance-to-digital converter series was developed precisely to address this task. With its band-pass characteristic and architecture, the circuit demonstrates an ability to withstand electromagnetic interference (EMI) effectively. The FDC2x1x series offers a narrowband design for interference resistance, high resolution, and high-speed operation support [37].

The capacitance sensor chip utilized in this design is the FDC2214 by Texas Instruments. It boasts a noise floor of 0.3 fF and a resolution of 28 bits. Operating within a supply voltage range of 3.3 V to 3.6 V, it can function across a temperature range of -40°C to 125°C . The chip supports high-precision capacitance detection by utilizing a differential single-channel mode. The STM32 microcontroller configures relevant registers via the IIC interface to achieve optimal testing results. The microcontroller receives and collects 24-bit raw data from the capacitance sensor, which are then transmitted via the serial-to-USB interface to the host computer for signal processing (with median filtering to reduce the sudden high-frequency noise) and display. The main control PCB and peripheral circuitry are illustrated in Figure 12. Shielded cables are employed to connect the main control PCB to the FPC electrodes to minimize interference. The shielding layer in the cables is grounded to reduce noise.

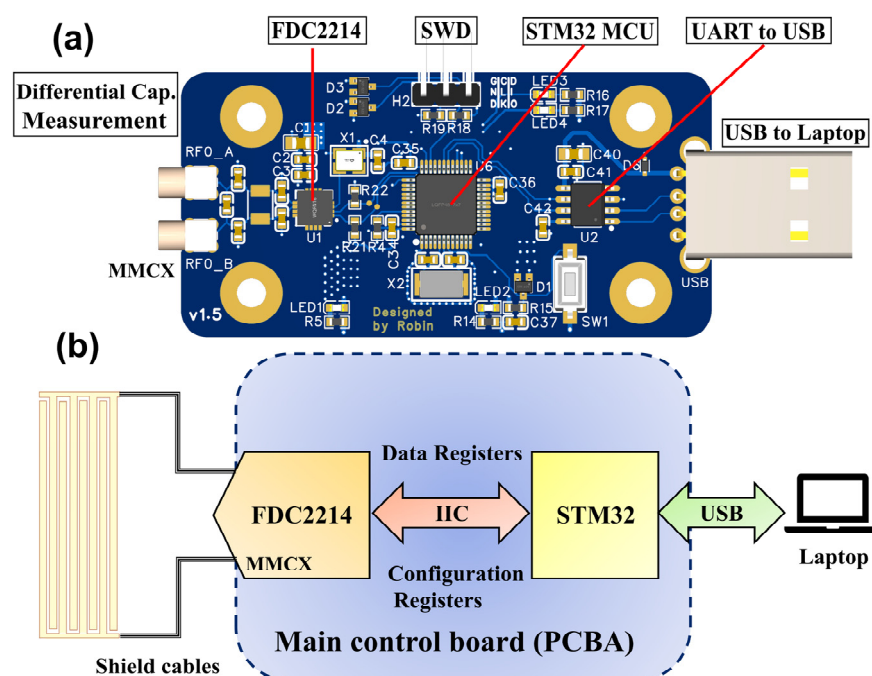


Figure 12. PCBA of the main control board in (a) 3D preview and (b) simplified diagram view.

The PCB is designed with four layers, featuring separate power and ground layers, thereby providing a complete return path for digital signals to maintain impedance consistency. The initial design of this sensor offers the following advantages:

1. Non-contact and non-intrusive: The flexible electrode of the sensor adheres to the outer surface of the test tube, enabling the detection of internal liquid changes without the need for contact or immersion. This approach effectively mitigates the risks associated with contamination and corrosion.
2. Versatility in container compatibility: The flexible substrate of the electrodes allows for adaptation to containers of various cross-sections and shapes. This feature enables the sensor to detect liquid level changes even in sealed, opaque containers, particularly in small-scale vessels.
3. Flexible calibration within the linear range: Zero and full-scale calibration lines can be dynamically adjusted, facilitating real-time, high-precision monitoring of continuous liquid level changes within the linear range.
4. Cost-effectiveness: The flexible material used for the electrodes incurs low production costs, and the manufacturing process is straightforward. Additionally, the sensor chip requires minimal BOM and is available at a low price.

The capacitance values of ceramic capacitors with different nominal values (with a 5% error margin) were measured using the capacitance sensor. A comparison was made with the measurements obtained from a Keysight LCR Meter, as detailed in Table 4. Here, the measured values indicate the difference between the sensor reading after connecting to the ceramic capacitor and the reading obtained from an empty measurement with only the cables. The LCR meter conducted tests with a 1 V AC and 1kHz excitation signal.

Table 4. Comparison of multiple measurement values between capacitive sensors and LCR.

Test Items	FDC Values (pF)	Measured Values (pF)	LRC Values (pF)	Relative Error
Sensor only	90.654	/	/	/
Senor with shield line	120.73	/	/	/
30 pF	150.98	30.25	30.1	0.50%
47 pF	166.56	45.83	46.15	0.70%
56 pF	176.88	56.15	55.6	0.90%
68 pF	188.35	67.62	67.06	0.80%
82 pF	201.73	81	80.71	0.30%
100 pF	218.93	98.2	97.1	1.10%

The testing ability of the capacitance measurement based on the FDC2214 for pF-level capacitors has been demonstrated to meet the standard.

5. Experimental Results and Discussion

The sensing electrode, with the exposed copper foil facing inward, is adhered to the outer surface of the test tube using double-sided adhesive tape. In order to ensure the consistency of the sensors' position between the experiment and the simulation, the IDT electrode is also at a height of 14 mm above the circular bottom of the cylinder of the test tube. Although previous studies have indicated that thinner tubes may result in higher sensitivity, the current tube available, which is 0.9 mm thick, limits the potential for further improvement. This is followed by the application of transparent tape to ensure complete fixation. The double-sided adhesive tape, comprising a PET substrate with a thickness of 0.01 mm, is suitable for curved surfaces and has been experimentally validated to enhance sensitivity compared to no adhesive. This is due to the fact that it ensures a snug fit between the sensing electrode and the test tube, thereby eliminating any air gaps. Two solder points on the electrode are soldered with shielded coaxial cables (with a diameter of 1.37 mm) terminated with MMCX connectors. One pair of differential interfaces of the capacitance measurement device is connected to the sensing electrode, while the other end is connected

to a laptop via USB. A Python program is employed to receive and process serial data from the microcontroller, converting 24-bit raw data into real-time capacitance data for display, thus facilitating continuous liquid level detection. Figure 13 illustrates the experimental setup, and all tests are conducted under ambient temperature conditions.

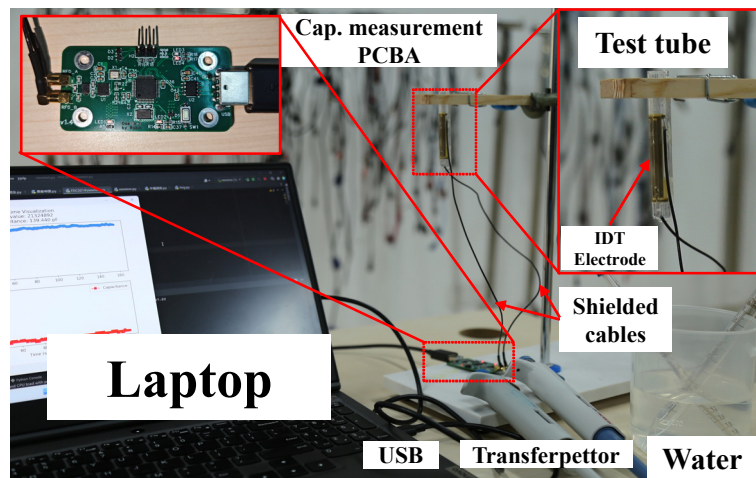


Figure 13. Experimental setup for non-contact capacitive sensing liquid level detection.

Pure water is added to the test tube until it covers the IDT electrode's lower edge. The capacitance data C_0 and height h_0 at the starting point are recorded ($h_0 = 14$ mm in this example). Subsequently, approximately 53 μL of water (raising the liquid level by 1 mm) is added to the test tube using a transferpettor, and the current capacitance data C , is recorded. It is recommended that a pipette be used to transfer the water into the test tube with precision each time in order to prevent the formation of a liquid film [38] on the inner wall of the test tube, which could affect the measurement. This process is repeated 40 times until the liquid level reaches the upper edge of the IDT electrode. It is important to note that the measured data represents the total capacitance within the entire circuit, including the sensing electrode, cables, and PCB parasitic parameters. In contrast, the simulated capacitance values only represent the capacitance of the sensing electrode. Before connecting the sensing electrode, the initial capacitance value of the test setup, including cables, is 120.758 pF. Therefore, the simulated values shown in Figure 14 are the results after adding the initial capacitance value of the device to the simulated values. Figure 14 illustrates the experimental test results compared to simulated values, including a reference fitting calibration line using the least squares method.

The test data shows that the capacitance values increase linearly with the rise in water level, confirming the theoretical prediction. The sensitivity $S = \Delta C / \Delta h = 78.68 \text{ fF/mm}$ of the fitting line or calibration curve, with an R-square value of 0.9996. The sensitivity of the simulated fitting line is 71 fF, with an R-square value of 0.9975. It is evident that the capacitance values and sensitivities of the actual test results closely match the simulated values. The average fitting error for the actual test values is only 22.4 fF, with a resolution of 1 mm.

Although the accuracy of simulation software is not absolute, the test results demonstrate a notable correlation between the actual and simulated data on the same coordinate axis. This verifies the high reliability of the simulation and provides insights and tools for subsequent optimization efforts.

Linearity, denoted by γ_L , represents the deviation between the actual curve and the fitting curve and is another essential indicator describing the static characteristics of the sensor. Linearity γ_L is defined as the maximum absolute deviation ΔL_{max} between the

actual curve and the fitting curve divided by the full-scale output γ_{FS} . In the effective measurement range, γ_{FS} is 3.06. It can be expressed as follows:

$$\gamma_L = \frac{\Delta L_{max}}{\gamma_{FS}} \times 100\% = \frac{0.05}{3.06} \times 100\% = 1.6\%. \quad (10)$$

It can be demonstrated that the sensor exhibits good linearity within the effective range of measurement.

Finally, the calculation for the real-time liquid level height h in the test tube is given by the following equation:

$$h = h_0 + \frac{C - C_0}{S}. \quad (11)$$

The capacitance values obtained from the tests are in exact correspondence (one-to-one) with the actual liquid level height. Furthermore, alterations to the experimental environment, such as changes to the solution or temperature, will influence the effects on both C and C_0 but will not affect the actual height of the h liquid level to be measured.

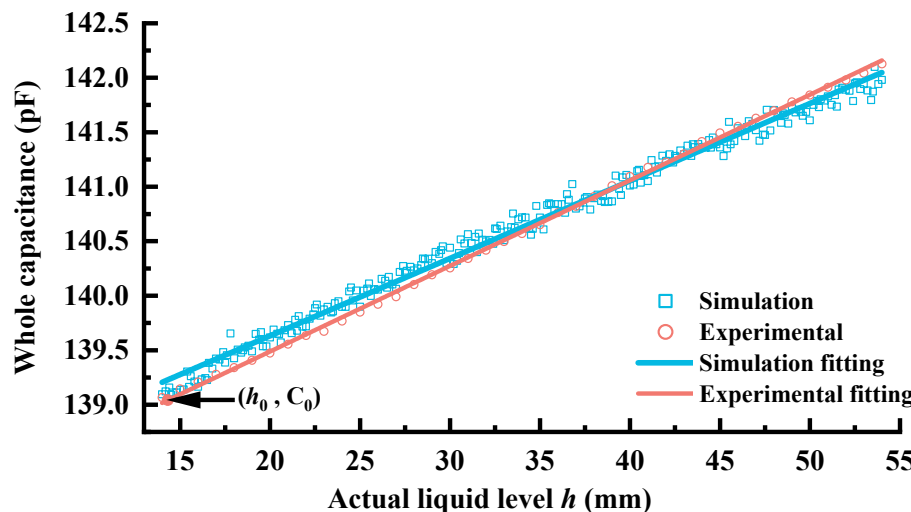


Figure 14. Comparison of the change in sensor capacitance relative to liquid level variation between simulated and measured values.

Figure 15 presents a comparison between the measured liquid level, converted according to Equation (11), and the actual liquid level, accompanied by an analysis of the errors between the two. The standard deviations of the calibration curve comparing the experimental data are shown in Figure 16.

Although the effective testing range is currently constrained by the height of the test electrode (40 mm), the linear characteristics observed and validated in both simulation and test data suggest the feasibility of increasing this height. Moreover, the flexible substrate material of the test electrode permits adaptation to a multitude of requirements for liquid level detection in containers of diverse shapes and capacities.

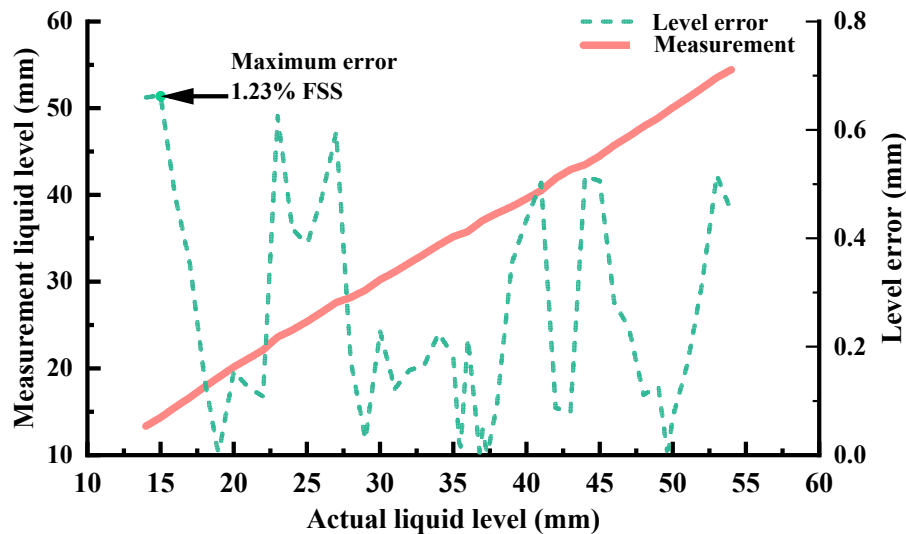


Figure 15. Comparison of measurement and experimental results with maximum error 1.23% full-scale span (FSS).

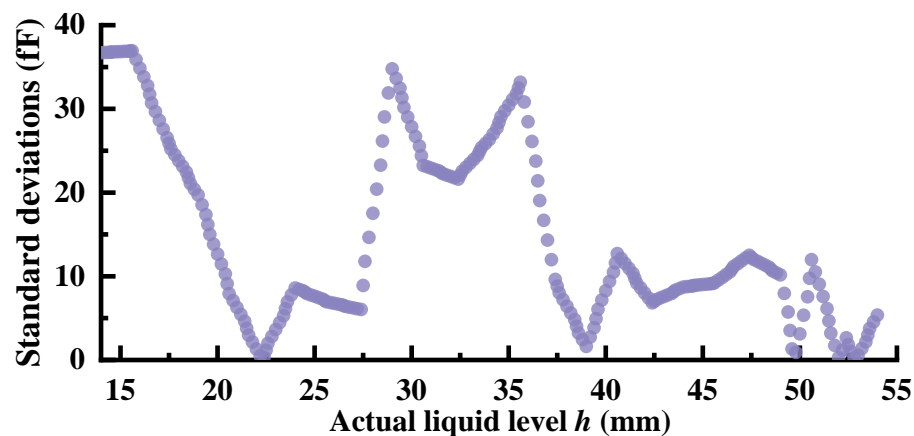


Figure 16. The standard deviations of the calibration curve.

6. Conclusions

This paper presents a novel capacitive IDT element-based FPC that has been designed and fabricated. The design employs a sensing electrode with a linear correlation between capacitance and liquid level within the effective range. The dimensions of the sensing electrode have been ascertained through a simulation tool. The simulation verified the conclusion that the thinner the wall of the glass test tube, the higher the sensitivity. This novel capacitive IDT element-based FPC presents a new approach for high-sensitivity measurement of liquid levels in test tubes, integrated with a capacitive detection and measurement circuit. The experimental results demonstrate that the sensor exhibits a high sensitivity characteristic of 78.68 fF/mm, which basically matches the simulation results. Furthermore, the sensor exhibits reliability, non-destructiveness, high linearity, and flexibility, rendering it suitable for a wide range of applications, particularly those involving tube-based sensing environments.

Nevertheless, further optimization is required in the design and manufacturing of the device to ensure its suitability for real-world production application scenarios. For instance, optimization and experimentation can be conducted on a range of container types and capacities. Furthermore, wireless features such as LoRa and low-power designs can be re-optimized and adapted to IoT-based liquid level sensor clusters for real-time monitoring and detection in railway tunnels, with some potential practical applications.

Author Contributions: Conceptualization, B.L. and Y.R.; methodology, B.L.; software, B.L. and X.F.; validation, Y.R., Y.S. and F.Y.; formal analysis, X.F.; investigation, B.L. and Z.F.; resources, Y.S.; data curation, B.L.; writing—original draft preparation, B.L.; writing—review and editing, B.L., Y.R. and F.Y.; visualization, Z.F.; supervision, F.Y.; project administration, F.Y.; funding acquisition, F.Y. All authors have read and agreed to the published version of the manuscript.

Funding: This research was funded by The Risk Identification and Digital Twin System Prototyping for Operational Safety of Guangzhou-Zhanjiang High-speed Railway 2023A0203602.

Data Availability Statement: Data are contained within the article.

Conflicts of Interest: The authors declare no conflicts of interest.

References

- Shin, J.; Lee, M.; Gupta, D.; Kim, S.; Gandla, S. Hydrogel-Based Real-Time Wireless Liquid Level Monitoring System for Size-Independent Infusion Bags. *Adv. Electron. Mater.* **2022**, *8*, 2200473. [[CrossRef](#)]
- Wei, Q.; Lee, J.H.; Seong, K.W.; Kim, M.N.; Cho, J.H. The design of a wireless flexible capacitive sensor detection system to detect liquid level in plastic bag intravenous drip sets. *Biomed. Eng. Lett.* **2011**, *1*, 247–253. [[CrossRef](#)]
- Oommen, B.; Philip, J. Soil moisture evaluation with spiral fringing field capacitive sensors. *Int. J. Environ. Sci. Technol.* **2024**, *21*, 3735–3746. [[CrossRef](#)]
- Kok, C.L.; Ho, C.K.; Tanjodi, N.; Koh, Y.Y. A Novel Water Level Control System for Sustainable Aquarium Use. *Electronics* **2024**, *13*, 2033. [[CrossRef](#)]
- Li, L.; Chen, H.; Huang, Y.; Xu, G.; Zhang, P. A new small leakage detection method based on capacitance array sensor for underground oil tank. *Process Saf. Environ. Prot.* **2022**, *159*, 616–624. [[CrossRef](#)]
- Yang, Y.; Hu, H.; Wang, K.; Wang, S.; Liu, M.; Zhang, C.; Wang, D. Area-alterable liquid electrode capacitance sensor for water holdup measurement in oil-water two-phase flow. *Asia-Pac. J. Chem. Eng.* **2021**, *16*, e2680. [[CrossRef](#)]
- Xu, Y.; Wang, Z. The study and implementation of connected liquid level detection technology applying to medical equipment. In Proceedings of the 2014 IEEE Workshop on Electronics, Computer and Applications, Ottawa, ON, Canada, 8–9 May 2014; pp. 333–336.
- Hanni, J.R.; Venkata, S.K. Does the existing liquid level measurement system cater the requirement of future generation? *Measurement* **2020**, *156*, 107594. [[CrossRef](#)]
- Lata, A.; Kumar, B.; Mandal, N. Design and development of a level transmitter using force resistive sensor as a primary sensing element. *IET Sci. Meas. Technol.* **2018**, *12*, 118–125. [[CrossRef](#)]
- Ding, Z.; Gong, W. Design of liquid level detection circuit based on sampling probe structure capacitance. *PLoS ONE* **2024**, *19*, e0298282. [[CrossRef](#)] [[PubMed](#)]
- Jin, B.; Zhang, Z.; Zhang, H. Structure design and performance analysis of a coaxial cylindrical capacitive sensor for liquid-level measurement. *Sens. Actuators A Phys.* **2015**, *223*, 84–90. [[CrossRef](#)]
- Hanni, J.R.; Venkata, S.K. A novel helical electrode type capacitance level sensor for liquid level measurement. *Sens. Actuators A Phys.* **2020**, *315*, 112283. [[CrossRef](#)]
- Chen, Q.; Chen, H.; Gao, Z.; Fan, X.; Wu, B.; Zhang, M.; Li, S. A liquid level optical fiber sensor with refractive index compensation through cascading double multi-mode interferences. *Infrared Phys. Technol.* **2022**, *127*, 104437. [[CrossRef](#)]
- Zhang, T.; He, X.; Liu, Y.; Li, B. Ultrasonic liquid level detection method based on the variation of reflected energy on the inner wall of a container. *Ultrasonics* **2024**, *139*, 107290. [[CrossRef](#)] [[PubMed](#)]
- Grassi, K.N.D.; Freire, R.C.S.; Villanueva, J.M.M. Evaluation of wavelet analysis performance in multiphase level measurement using ultrasonic sensors. In Proceedings of the 2014 IEEE International Instrumentation and Measurement Technology Conference (I2MTC) Proceedings, Montevideo, Uruguay, 12–15 May 2014; pp. 756–760.
- Kossenas, K.; Podilchak, S.K.; Beveridge, M. A microwave liquid level determination method for oil and gas pipelines. *IEEE Access* **2022**, *10*, 67031–67046. [[CrossRef](#)]
- El-Nady, S.; Afifi, A.; El-Hameed, A.; Anwer, S. Sugar and Salt Concentration Detection in Water Employing ENZ Metamaterial Microwave Sensor. *Wirel. Pers. Commun.* **2024**, *134*, 189–208. [[CrossRef](#)]
- Xu, X.; Li, Z.; Li, G.; Li, J.; Wen, C. An acoustic resonance-based liquid level detector with error compensation. *IEEE Trans. Instrum. Meas.* **2018**, *68*, 963–971. [[CrossRef](#)]
- Cravotto, G.; Cintas, P. The combined use of microwaves and ultrasound: Improved tools in process chemistry and organic synthesis. *Chem.—A Eur. J.* **2007**, *13*, 1902–1909. [[CrossRef](#)] [[PubMed](#)]
- Bobovnik, G.; Mušić, T.; Kutin, J. Liquid level detection in standard capacity measures with machine vision. *Sensors* **2021**, *21*, 2676. [[CrossRef](#)]
- Jilun, Z.; Yi, Z.; Ying, L.; Fang, C.; Ying, L.; Hong, Q. Non-contact Liquid Level Detection Method Based on Multilayer Spiking Neural Network. *J. Electron. Inf. Technol.* **2023**, *45*, 2759–2769.

22. Islam, T.; Maurya, O.P. Design and fabrication of non-contact fringing field capacitive sensor for liquid level measurement. In Proceedings of the 2019 IEEE 16th India Council International Conference (INDICON), Rajkot, India, 13–15 December 2019; pp. 1–4.
23. Ahmad, S.; Khalid, N.; Mirzavand, R. Detection of soil moisture, humidity, and liquid level using CPW-based interdigital capacitive sensor. *IEEE Sens. J.* **2022**, *22*, 10338–10345. [[CrossRef](#)]
24. Qian, Z.; Li, T.; Kim, S.; Cheng, Y.-J.; Sakthivelpathi, V.; Chung, J.-H. Liquid level measurement using a single electrode capacitive sensor made of carbon nanotube-paper composite. *Phys. Scr.* **2024**, *99*, 045963. [[CrossRef](#)]
25. Tang, Z.; Tao, Z.; Cao, Y.; Zhang, Q.; Liu, W.; Cao, C. Capacitively coupled contactless conductivity detection-based sensor for liquid level measurement and application to clinical infusion monitoring. *Sens. Actuators A Phys.* **2024**, *367*, 115073. [[CrossRef](#)]
26. Ahmad, S.; Khosravi, R.; Iyer, A.K.; Mirzavand, R. Wireless capacitive liquid-level detection sensor based on zero-power RFID-sensing architecture. *Sensors* **2022**, *23*, 209. [[CrossRef](#)] [[PubMed](#)]
27. Islam, T.; Maurya, O.P.; Khan, A.U. Design and fabrication of fringing field capacitive sensor for non-contact liquid level measurement. *IEEE Sens. J.* **2021**, *21*, 24812–24819. [[CrossRef](#)]
28. Hu, X.; Yang, W. Planar capacitive sensors—designs and applications. *Sens. Rev.* **2010**, *30*, 24–39. [[CrossRef](#)]
29. Zhu, Y.; Zhou, R.; Zhang, Y.; Dong, X.; Huang, X. Review on flashover risk prediction method of iced insulator based on icing monitoring technology. *Cold Reg. Sci. Technol.* **2021**, *185*, 103252. [[CrossRef](#)]
30. Jiao, J.; Li, L.; He, C.; Wu, B. Design of Improved Interdigital Capacitive Proximity Sensor Used for Dielectric Property Detection of Thickness Gradual Changed Structure. *J. Mech. Eng.* **2017**, *53*, 1–9. [[CrossRef](#)]
31. Yossontikul, C.; Ungpinitpong, P.; Chitsakul, K.; Sangworasil, M. A comparative study of capacitance image reconstruction. In Proceedings of the 2003 IEEE Pacific Rim Conference on Communications Computers and Signal Processing (PACRIM 2003) (Cat. No. 03CH37490), Victoria, BC, Canada, 28–30 August 2003; pp. 1024–1027.
32. Vakilian, M.; Majlis, B.Y. Study of interdigitated electrode sensor for lab-on-chip applications. In Proceedings of the 2014 IEEE International Conference on Semiconductor Electronics (ICSE2014), Kuala Lumpur, Malaysia, 27–29 August 2014; pp. 201–204.
33. Igreja, R.; Dias, C. Analytical evaluation of the interdigital electrodes capacitance for a multi-layered structure. *Sens. Actuators A Phys.* **2004**, *112*, 291–301. [[CrossRef](#)]
34. Mamishev, A.V.; Sundara-Rajan, K.; Yang, F.; Du, Y.; Zahn, M. Interdigital sensors and transducers. *Proc. IEEE* **2004**, *92*, 808–845. [[CrossRef](#)]
35. Claudel, J.; Alves de Araujo, A.; Kourtiche, D.; Nadi, M.; Bourjilat, A. Optimization of interdigitated sensor characteristics. In *Interdigital Sensors: Progress over the Last Two Decades*; Springer: Cham, Switzerland, 2021; pp. 91–122.
36. Alveringh, D.; Groenesteijn, J.; Wiegerink, R.J.; Lötters, J. Improved capacitive detection method for Coriolis mass flow sensors enabling range/sensitivity tuning. *Microelectron. Eng.* **2016**, *159*, 1–5. [[CrossRef](#)]
37. Huang, K.; Zhang, Z. Algorithm Research for Bubble Detection in Capacitive Liquid Level Sensor of Fully Automated Immunoassay Analyzer. *J. Phys. Conf. Ser.* **2023**, *2637*, 012034. [[CrossRef](#)]
38. Chetpattananondh, K.; Tapoanoi, T.; Phukpattaranont, P.; Jindapetch, N. A self-calibration water level measurement using an interdigital capacitive sensor. *Sens. Actuators A Phys.* **2014**, *209*, 175–182. [[CrossRef](#)]

Disclaimer/Publisher’s Note: The statements, opinions and data contained in all publications are solely those of the individual author(s) and contributor(s) and not of MDPI and/or the editor(s). MDPI and/or the editor(s) disclaim responsibility for any injury to people or property resulting from any ideas, methods, instructions or products referred to in the content.